ESKİŞEHİR TECHNICAL UNIVERSITY JOURNAL OF SCIENCE AND TECHNOLOGY
A- APPLIED SCIENCES AND ENGINEERING

2022, 23(3), pp. 223-232, DOI:10.18038/estubtda.1149416

RESEARCH ARTICLE

# CHARACTERIZATION OF ARTIFICIALLY GENERATED 2D MATERIALS USING CONVOLUTIONAL NEURAL NETWORKS

**Cahit PERKGÖZ [1], Mehmet Zahit ANGİ [1]**

[1] Department of Computer Engineering, Faculty of Engineering, Eskişehir Technical University, Eskişehir, Turkey

## ABSTRACT

Two dimensional (2D) materials have attracted many researchers due to the high-performance of the devices produced by these materials. There are different methods to produce 2D materials such as wet chemical synthesis, chemical vapor deposition (CVD), molecular beam epitaxy, atomic layer deposition, pulsed laser deposition (PLD), all of which require hours during the processes. Once the 2D structures are obtained, their properties including their defects should be revealed by different characterization tools. Characterization process also requires time and expertise. In this respect, deep learning methods such as Convolutional Neural Networks (CNN) can be a solution for the practical and rapid classification of the produced samples. However, there is not enough number of samples in most of the research laboratories because of the above-mentioned long experimental processes. This work presents the performance of a CNN algorithm using artificially created images of $MoS_2$, a commonly studied 2D semiconductor with a high potential in different electronics applications. The synthetic optical microscopic images including normal and defected $MoS_2$ flakes are generated by the intensities of light incident on different materials using Fresnel Equations. A deep CNN algorithm is constructed to detect the normal and defective samples. As a result of the experiments, an average of 88.9% accuracy was obtained. These results can be interpreted that CNN can be used in the future for the characterization of two-dimensional materials with a sufficient number of real images.

**Keywords:** $MoS_2$, Two-dimensional Materials, Fresnel Equations, Characterization, Deep Learning

## 1. INTRODUCTION

The scaling-down in transistors has led to great progress in silicon-CMOS technology. Reducing the physical dimensions at the beginning of the technology development resulted in an improvement in speed performance where the power density did not change much. However, in recent years, voltage scaling had to be carefully considered, given that lowering the threshold voltage makes it difficult to drive enough current, which means an increase in leakage current [1]. Remembering that there is the fundamental limit of subthreshold swing (SS), which has to be larger than 60 mV per decade at 300 K in conventional MOSFETs [2], the power density power in high-performance microprocessors is demanding complicated power management methods although reduction of physical dimensions has still been carried out up to present [3]. The problems related to the rise of static power and the leakage of current between the source and drain electrodes are examined under the concept of short-channel effects. In this sense, novel and smart strategies have to be pursued to overcome the aforementioned limitations and continue to improve the performance of transistors.

At this point, FETs that are made up of a 2 dimensional (2D) material based channel do not suffer from leakage current since the electrons are confined in atomically thin layers where the gate voltage provides a uniform operation [4]. Hence, lately, the potential of layered materials, namely 2D materials, have been recognized for advanced technological applications [5]. Such 2D materials present unusual properties that do not exist unconventional bulk materials. The most widely studied 2D material is

*Corresponding Author: cahitperkgoz@eskisehir.edu.tr
Received: 27.07.2022 Published: 27.09.2022

graphene [6], which is a sheet of carbon atoms atomically thin where its pristine form has a zero-bandgap and is counted as a semimetal. However, the lack of an energy bandgap makes graphene unsuitable for FET applications, despite different efforts to open a bandgap. Therefore, other 2D materials have started to come into play, mainly semiconductor transition metal dichalcogenides (TMDs) as they possess a bandgaps in the visible and infrared spectral range. On the other hand, there are still critical challenges related to production and characterization of these 2D materials to be utilized as a compelling technology.

Chronologically, first 2D materials were realized by using mechanical exfoliation, which were limited to some tens of micrometers [7]. Other methods such as wet chemical synthesis, chemical vapor deposition (CVD), molecular beam epitaxy, atomic layer deposition, pulsed laser deposition (PLD) have been studies to realize such 2D materials [8], where among these, the CVD process has advanced in years and it is recognized as a high potential technique that can provide scalable 2D materials [9, 10] and it is well-suited with microelectronic processes [11]. Nevertheless, the activation of gaseous reactions , controllability of the formed structures and wafer-size fabrication persist as critical issues [12]. In addition to these, 2D material characterization includes time-consuming and sometimes expensive routes such as Raman scattering spectroscopy, atomic force microscopy (AFM), photoluminescence (PL) spectroscopy, which are not suitable for large-area analysis [13, 14]. If the usage of an optical microscope is enhanced also as a tool to understand the uniformity and layer thickness then such a practical and low-cost option of characterization tool would make significant contribution to the field considering that mainly, an optical microscope is the first tool that is utilized to investigate the obtained 2D materials [15].

CVD grown 2D materials can include different number of layers, defects, gain boundaries, wrinkles and oxide formations, which can affect the device operation of a device of which the active region is made up of 2D materials. Hence, recently, there are ongoing researches that utilize a relatively simple characterization tool, optical microscope, to make detailed analyses of 2D materials while still keeping rapidness and large-area examination where these techniques engage deep learning-based methods is established on artificial neural networks [16-18].

There is an increasing usage of these artificial intelligence techniques in diverse fields including medicine, diagnosis, biology, physics, and electronics [19-22]. Image processing, classification, clarifying and creating images are also among the other applications [23]. Out of various deep learning methods, convolutional neural networks (CNN) out-performs other techniques for image identification and arrangement [24-26].

This article mainly focuses on obtaining a method to decide if CVD grown 2D TMD materials, namely $MoS_2$ monolayers, are suitable to be employed in devices such as transistors, sensors or detectors. Such formations will be referred as intact structures hereafter. In this study, a deep learning method for the characterization of 2D $MoS_2$ will be applied where artificial images, which mimic the images that are obtained by optical microscopy tool, are produced using Fresnel equations for training and testing.

## 2. METHODS

### 2.1. Fresnel Equations

Light, as an electromagnetic wave, incident on a surface is partially reflected and partially refracted. According to the Snell's law, the reflection and transmission angles of these waves can be calculated. Based on these angles, Fresnel equations, which define the ratio of the electric field of reflected and refracted waves, are derived [27, 28]. A bright-field microscope creates images by using the contrast of the reflected light from the different points of the sample surface. Therefore, generating synthetic images could be possible if the physical properties of both the substrates and the deposited materials are known.

The cross section of a sample for a typically grown 2D material to be examined under the optical microscope is given below.

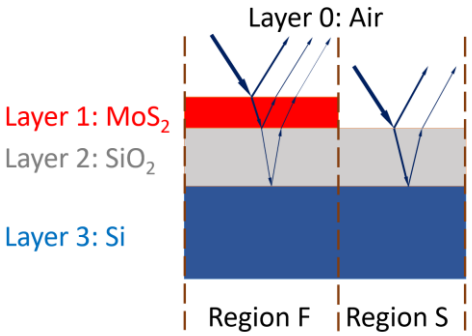


**Figure 1.** Cross-section of a grown 2D material ($MoS_2$).

The optical contrast of the sample for two regions can be defined as in Equation 1.

$$C = \frac{I_F - I_S}{I_F + I_S} \tag{1}$$

where $I_F$ and $I_S$ are the light intensities in region *F* and region *S*, respectively. As it is shown in Figure 1, region *F* has a 2D material ($MoS_2$) on the substrate ($SiO_2$/Si), whereas region *S* has only the substrate ($SiO_2$/Si). Therefore, light intensities reflected by two different regions would be different and can be defined as:

$$I_F = |\bar{r}_F r_F| \tag{2}$$
$$I_S = |\bar{r}_S r_S| \tag{3}$$

where, $r_F$ and $r_S$ are the reflection Fresnel coefficients for region *F* and *S*, respectively. These two values should be analyzed for two cases where in region *S* there is only the substrate (3 layers including air, $SiO_2$ and Si) and in region *F* the substrate is covered with the 2D material (4 layers including air, $MoS_2$, $SiO_2$ and Si). The related reflection Fresnel coefficients for the regions are defined as in Equation 4 and 5.

$$r_F = \frac{r_{01}e^{i(\emptyset_1+\emptyset_2)} + r_{12}e^{-i(\emptyset_1-\emptyset_2)} + r_{23}e^{-i(\emptyset_1+\emptyset_2)} + r_{01}r_{12}r_{23}e^{i(\emptyset_1-\emptyset_2)}}{e^{i(\emptyset_1+\emptyset_2)} + r_{01}r_{12}e^{-i(\emptyset_1-\emptyset_2)} + r_{01}r_{23}e^{-i(\emptyset_1+\emptyset_2)} + r_{12}r_{23}e^{i(\emptyset_1-\emptyset_2)}} \tag{4}$$

$$r_S = \frac{r_{01} - r_{12}e^{-i2\emptyset_1}}{1 + r_{01}r_{12}e^{-i2\emptyset_1}} \tag{5}$$

where, Fresnel coefficients ($r_{ij}$) are the functions of refractive indexes ($n_i$ and $n_j$) of the overlapping layers *i* and *j*:

$$r_{ij} = \frac{(n_i - n_j)}{(n_i + n_j)} \tag{6}$$

and $\emptyset_i$ is the phase shift resulted by the propagation of the light in the medium of layer *i*. $\emptyset_i$ is expressed as:

$$\emptyset_i = \frac{2\pi n_i d_i}{\lambda} \tag{7}$$

where $n_i$, $d_i$ and $\lambda$ are the refractive index, the thickness of the medium $i$, and the wavelength of the light, respectively. The index $i$ is 0 for air, 1 for $MoS_2$, 2 for $SiO_2$ and 3 for Si.

Hence, for an artificially created structure shown in Figure 1 with the specific values of the refractive indices of the media, the intensities of light for the two regions can be obtained under different wavelengths. Then, an artificial RGB image can be constructed for different thicknesses from which the 2D material can be characterized.

### 2.2. Convolutional Neural Networks

Hubel and Wiesel discovered "simple cells" and "complex cells" regarding the kitten visual cortex in 1959 [29]. According to this study, two kinds of cells are used for visual recognition. 20 years later, this study gave inspiration to Kunihiko Fukushima where the artificial neural network was designed to mimic such complex and simple cells [30]. The artificial cells were evidently not biological neurons, but rather mathematical operations. Fukushima's model was detecting simple shapes by simple cells whereas complex images (e.g., a human face) by complex cells which use lower-level complex cells or simple cells to get the features (e.g., an eye). In the 1990s, first modern convolution neural networks published by Yann LeCun [31]. In this research, LeCun created a convolutional neural network to recognize handwritten characters from the dataset which is called MNIST.

A CNN is a structure/concept that typically has three types of layers: convolution layer, pooling layer, and fully connected layer (Figure 2). The convolution layer and the pooling layer extract the features, and the fully connected layer is a typical neural network which maps the flattened layer vector to the output. Convolution layers perform convolution operation by some numbers of filters (kernels). Pixel values in digital images are processed by a kernel, a feature extractor. As you move through the layers, the extracted features also move from low-level to high-level patterns.

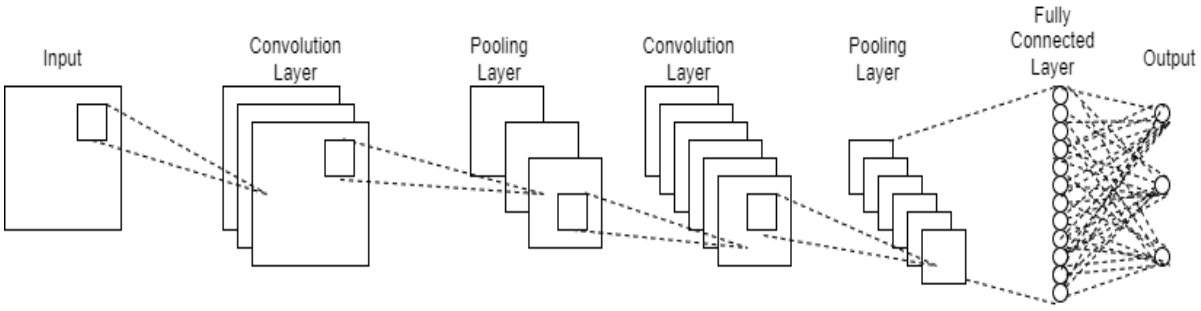


**Figure 2.** Convolutional Neural Network

### Input Layer

The first layer of the CNN is the input layer from which the network receives the data raw data. The data size sent to this layer is critical for to the successful implementation of the model being intended. Choosing an image size rather large at the input increases high storage requirements as well as training and testing time per image. Furthermore, it can improve the network success rate. Choosing a smaller input image size can reduce memory requirements and reduce the training time. However, this time, smaller input image size will cause the depth of the network to decrease and the performance to deteriorate. Hence, for analyzing images, it is of importance to choose a proper image size in the input to reach the appropriate network depth, network success rate, and hardware computational cost.

**Convolution Layer**

The basis of the CNN is the convolution layer also recognized as the transformation level. This conversion process is built on looping specific filters throughout the full image. Therefore, a layered architecture comprises filters that are an integral part of the architecture with different filter sizes. Filters generate output data by means of employing a convolution operation to the preceding level image. Accordingly, this convolution operation provides the feature maps to be formed. The map of activation is the area where specific features are found for each filter. While training a CNN in the training set, each learning iteration changes the coefficients of these filters. In this way, the network can determine which areas of the data are essential for representation.

In case that we come up with some $M \times N$ size input ($I$) for any convolution operation and use an $m \times n$ filter "$f$" the size of the convolutional layer output $X$ will become $(M-m+1) \times (N-n+1)$ and can be obtained by the following Equation.

$$X_{i,j} = \sum_{b=0}^{N-1} \sum_{a=0}^{M-1} W_{(i+a-1),(j+b-1)} f_{a,b} \tag{8}$$

**Pooling Layer**

The main objective of this layer is to decrease the input size for the next layer. The size of the depth is not changed by pooling operation. The process executed at this layer can be called "downsampling". The information loss due to the reduction size would provide two advantages. Firstly, it decreases the simulation time resulting from a smaller number of parameters in the network. Secondly, overfitting problem is avoided in deep learning. Although pooling operation is held by so called filters, this operates differently from the filters in convolution layer. For example, max pooling is that taking the maximum value of a group of pixels defined initially.

**Fully Connected Layer**

In a CNN architecture, after the successive convolution and pooling layers are completed, fully connected layers need to be considered. This layer takes inputs from the last pooling layer which are flattened. The number of hidden layers will vary in different architectures. Each neuron in each layer is fully connected to the previous and next layer neurons. Hence, this layer is called a fully connected layer. If the input of fully connected layer is represented by a vector $h$, layer number by $l$, neuron weights by a matrix $W$ and bias vector by $B$, then the input of transfer function ($\sigma$) and the output of the layer will be defined as:

$$h^{in}{}_l = W_l \, h_{l-1}^{out} + B_l \tag{9}$$

$$y_l = \sigma(h^{in}{}_l) \tag{10}$$

**Output Layer**

This layer is the last layer of the fully connected layer. Classification happens at this level of this deep learning architecture. The output value of this layer is equal to the number of objects to be classified. Various transfer functions can be used in this layer.

## 3. RESULTS and DISCUSSIONS

The CNN algorithm developed for the classification of normal and defective stamps uses 10,000 artificial images of 100x100 pixels where 60% of the dataset is reserved for training, 20% for validation and 20% for testing. Half of the images contain normal flakes and the rest have distorted $MoS_2$ flakes. Distorted scales consist of two or more layers or have irregular structures. The images are created based on the intensity values for region *F* and *S* under red, green and blue light. For a normal flake, which has only one layer of $MoS_2$, $d_1 = 0.63$ nm [32]. The thickness of $SiO_2$ ($d_2$) is 300 nm [32]. The refractive indices $n_i$ are given in Table 1 below for the colors in red, green, and blue [32].

**Table 1.** Refractive Indices

| $n$ | Red | Green | Blue |
|---|---|---|---|
| $n_1$($MoS_2$) | 4.3-1$i$ | 4.0-0.6$i$ | 4.5-1$i$ |
| $n_2$ ($SiO_2$) | 1.2 | 1.29 | 1.36 |
| $n_3$ (Si) | 3.84-0.016$i$ | 4.04-0.03$i$ | 4.67-0.14$i$ |

Based on the above parameters and Fresnel equations given in Section 2, the intact flakes are created and placed randomly on the images. For the case of defected flakes, non-uniform $MoS_2$ structures are created for various $d_1$values which will be multiples of one-layer $MoS_2$ thickness. Some examples for both of the cases are given in Figure 3.

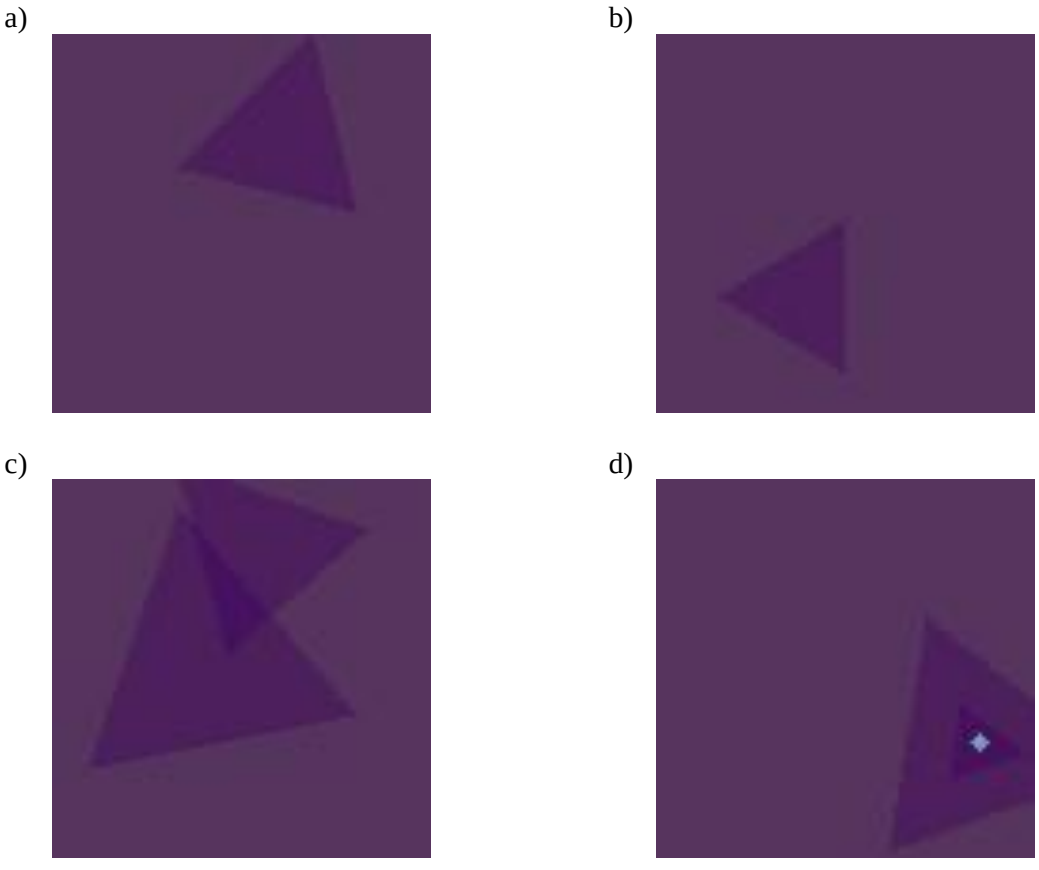


**Figure 3**. a, b) Intact flakes, c, d) defected flakes

In order to classify the uniformly and defected grown 2D materials, the CNN is structured as follows: There are 4 convolution layers where the convolution operation is held by 8, 16, 32 and 64 number of filters with 7x7, 7x7, 5x5 and 3x3 sizes, respectively. The pooling operation is held by choosing the

maximum of 2x2 pixels after each convolution layer. All the neurons in the network have LeakyRELU transfer function, except for the output neuron. A LeakyRELU transfer function is given in Figure 4.

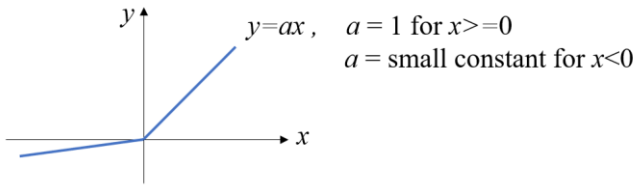


**Figure 4**. LeakyRELU Transfer Function

The output of the last maxpooling layer is flattened, which is the input vector of the fully connected layer of size 576. The fully connected layer has 64 neurons in the hidden layer and one output neuron with a sigmoid transfer function. The adaptive moment estimation (ADAM) optimizer is applied with a learning rate of 0.1.

The CNN algorithm is simulated 10 times with the same data set and the parameters on a PC computer which has a 3.5 GHz processor, of 128 GB RAM memory and RTX A5000 GPU. The created data has two classes of equal number of images. Performance metrics given in Equation 11-14 are used to find out the success of the CNN algorithm.

$$Accuracy = \frac{TP + TN}{TP + TN + FP + FN} \times 100 \tag{11}$$

$$Precision = \frac{TP}{TP + FP} \times 100 \tag{12}$$

$$Recall = \frac{TP}{TP + FN} \times 100 \tag{13}$$

$$F_1 Score = 2 \times \frac{Precision \times Recall}{Precision + Recall} \tag{14}$$

where, TP is the true positives, TN is the true negatives, FP is the false positives and FN is the false negatives.

The proposed method is simulated 10 times with the same parameters and the same data set. After obtaining the trained CNN structure, the test data is evaluated additionally. The performance metrics are obtained as given in Table 2 for the test data.

**Table 2.** Performance Metrics

| Accuracy | Precision | Recall | $F_1$ Score |
|---|---|---|---|
| 88.9% | 89.8% | 88.1% | 88.9% |

## 4. CONCLUSIONS

The production and characterization of nanomaterials is a time-consuming and demanding process, which required an expert to analyze and interpret the results. However, a CNN based deep learning method can do this laborious task in a very short time if it can be trained with a sufficient number of samples. In this work, first of all, 2D materials are created by using Fresnel equations and the material-specific values to obtain enough amount of data. The images of the flakes are constructed artificially assuming that a $MoS_2$ flake is on a $SiO_2$ layer which lays on a Si substrate. The intensity values of a normal light are calculated for both the regions with and without $MoS_2$ layer. From the intensity values the images are obtained for two classes of samples, based on the most encountered sample images. Then, a CNN structure is proposed to determine whether the sample is intact or defected. The classification performance of a CNN is evaluated by using these artificially created microscopic images that include two dimensional materials. Even though the images were artificially created, the high accuracy of the results have proved that CNN algorithms can also be used in the future with sufficient number of experimentally obtained data. Also, this work can be carried out for different types of 2D materials for the classification of intact and defected samples.

## ACKNOWLEDGEMENTS

This work was supported by Eskişehir Technical University Scientific Research Projects Commission under the grant no: 22ADP144.

## CONFLICT OF INTEREST

The authors stated that there are no conflicts of interest regarding the publication of this article.

## REFERENCES

[1] Chang L, Frank DJ, Montoye RK, Koester SJ, Ji BL, Coteus PW, et al. Practical strategies for power-efficient computing technologies. Proceedings of the IEEE. 2010;98:215-36.

[2] Park JH, Jang GS, Kim HY, Seok KH, Chae HJ, Lee SK, et al. Sub-kT/q subthreshold-slope using negative capacitance in low-temperature polycrystalline-silicon thin-film transistor. Scientific reports. 2016;6:1-9.

[3] Attia KM, El-Hosseini MA, Ali HA. Dynamic power management techniques in multi-core architectures: A survey study. Ain Shams Engineering Journal. 2017;8:445-56.

[4] Chhowalla M, Jena D, Zhang H. Two-dimensional semiconductors for transistors. Nature Reviews Materials. 2016;1:1-15.

[5] Kong W, Kum H, Bae S-H, Shim J, Kim H, Kong L, et al. Path towards graphene commercialization from lab to market. Nature nanotechnology. 2019;14:927-38.

[6] Novoselov KS, Geim AK, Morozov SV, Jiang D-e, Zhang Y, Dubonos SV, et al. Electric field effect in atomically thin carbon films. science. 2004;306:666-9.

[7] Yi M, Shen Z. A review on mechanical exfoliation for the scalable production of graphene. Journal of Materials Chemistry A. 2015;3:11700-15.

[8] Bonaccorso F, Lombardo A, Hasan T, Sun Z, Colombo L, Ferrari AC. Production and processing of graphene and 2d crystals. Materials Today. 2012;15:564-89.

[9] Zhang Y, Yao Y, Sendeku MG, Yin L, Zhan X, Wang F, et al. Recent progress in CVD growth of 2D transition metal dichalcogenides and related heterostructures. Advanced materials. 2019;31:1901694.

[10] Aras FG, Yilmaz A, Tasdelen HG, Ozden A, Ay F, Perkgoz NK, et al. A review on recent advances of chemical vapor deposition technique for monolayer transition metal dichalcogenides ($MX_2$: Mo, W; S, Se, Te). Materials Science in Semiconductor Processing. 2022;148:106829.

[11] Liu D, Chen X, Yan Y, Zhang Z, Jin Z, Yi K, et al. Conformal hexagonal-boron nitride dielectric interface for tungsten diselenide devices with improved mobility and thermal dissipation. Nature communications. 2019;10:1188.

[12] Lin Z, McCreary A, Briggs N, Subramanian S, Zhang K, Sun Y, et al. 2D materials advances: from large scale synthesis and controlled heterostructures to improved characterization techniques, defects and applications. 2D Materials. 2016;3:042001.

[13] Özden A, Şar H, Yeltik A, Madenoğlu B, Sevik C, Ay F, et al. CVD grown 2D $MoS_2$ layers: A photoluminescence and fluorescence lifetime imaging study. physica status solidi (RRL)–Rapid Research Letters. 2016;10:792-6.

[14] Zhang J, Yu Y, Wang P, Luo C, Wu X, Sun Z, et al. Characterization of atomic defects on the photoluminescence in two‐dimensional materials using transmission electron microscope. InfoMat. 2019;1:85-97.

[15] Yorulmaz B, Özden A, Şar H, Ay F, Sevik C, Perkgöz NK. CVD growth of monolayer $WS_2$ through controlled seed formation and vapor density. Materials Science in Semiconductor Processing. 2019;93:158-63.

[16] Lin X, Si Z, Fu W, Yang J, Guo S, Cao Y, et al. Intelligent identification of two-dimensional nanostructures by machine-learning optical microscopy. Nano Research. 2018;11:6316-24.

[17] Saito Y, Shin K, Terayama K, Desai S, Onga M, Nakagawa Y, et al. Deep-learning-based quality filtering of mechanically exfoliated 2D crystals. npj Computational Materials. 2019;5:1-6.

[18] LeCun Y, Bengio Y, Hinton G. Deep learning. nature. 2015;521:436-44.

[19] Shinde PP, Shah S. A Review of Machine Learning and Deep Learning Applications. 2018 Fourth International Conference on Computing Communication Control and Automation (ICCUBEA)2018. p. 1-6.

[20] Shorten C, Khoshgoftaar TM, Furht B. Deep Learning applications for COVID-19. Journal of Big Data. 2021;8:1-54.

[21] Masubuchi S, Machida T. Classifying optical microscope images of exfoliated graphene flakes by data-driven machine learning. npj 2D Materials and Applications. 2019;3:1-7.

[22] Bharati S, Podder P, Mondal M. Artificial neural network based breast cancer screening: a comprehensive review. arXiv preprint arXiv:200601767. 2020.

[23] Masubuchi S, Watanabe E, Seo Y, Okazaki S, Sasagawa T, Watanabe K, et al. Deep-learning-based image segmentation integrated with optical microscopy for automatically searching for two-dimensional materials. npj 2D Materials and Applications. 2020;4:1-9.

[24] Yao G, Lei T, Zhong J. A review of convolutional-neural-network-based action recognition. Pattern Recognition Letters. 2019;118:14-22.

[25] Alzubaidi L, Zhang J, Humaidi AJ, Al-Dujaili A, Duan Y, Al-Shamma O, et al. Review of deep learning: Concepts, CNN architectures, challenges, applications, future directions. Journal of big Data. 2021;8:1-74.

[26] Bhuvaneswari V, Priyadharshini M, Deepa C, Balaji D, Rajeshkumar L, Ramesh M. Deep learning for material synthesis and manufacturing systems: a review. Materials Today: Proceedings. 2021;46:3263-9.

[27] Blake P, Hill E, Castro Neto A, Novoselov K, Jiang D, Yang R, et al. Making graphene visible. Applied physics letters. 2007;91:063124.

[28] Zhang W, Zhao Q, Puebla S, Wang T, Frisenda R, Castellanos-Gomez A. Optical microscopy–based thickness estimation in thin GaSe flakes. Materials Today Advances. 2021;10:100143.

[29] Hubel DH, Wiesel TN. Receptive fields of single neurones in the cat's striate cortex. The Journal of physiology. 1959;148:574.

[30] Fukushima K, Miyake S. Neocognitron: A self-organizing neural network model for a mechanism of visual pattern recognition. Competition and cooperation in neural nets: Springer; 1982. p. 267-85.

[31] LeCun Y, Bottou L, Bengio Y, Haffner P. Gradient-based learning applied to document recognition. Proceedings of the IEEE. 1998;86:2278-324.

[32] Refractive index database https://refractiveindex.info/